Journal Pre-proof

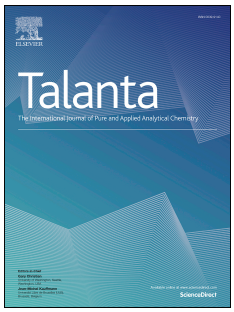

Highly selective impedimetric determination of *Haemophilus influenzae* protein D using maze-like boron-doped carbon nanowall electrodes

Mateusz Brodowski, Marcin Kowalski, Marta Skwarecka, Katarzyna Pałka, Michał Skowicki, Anna Kula, Tomasz Lipiński, Anna Dettlaff, Mateusz Ficek, Jacek Ryl, Karolina Dziąbowska, Dawid Nidzworski, Robert Bogdanowicz

PII: S0039-9140(20)30914-0

DOI: https://doi.org/10.1016/j.talanta.2020.121623

Reference: TAL 121623

To appear in: *Talanta*

Received Date: 25 May 2020

Revised Date: 27 August 2020

Accepted Date: 31 August 2020

Please cite this article as: M. Brodowski, M. Kowalski, M. Skwarecka, K. Pałka, M. Skowicki, A. Kula, T. Lipiński, A. Dettlaff, M. Ficek, J. Ryl, K. Dziąbowska, D. Nidzworski, R. Bogdanowicz, Highly selective impedimetric determination of *Haemophilus influenzae* protein D using maze-like boron-doped carbon nanowall electrodes, *Talanta*, https://doi.org/10.1016/j.talanta.2020.121623.

Highly selective impedimetric determination of *Haemophilus influenzae* protein D using maze-like boron-doped carbon nanowall electrodes

Mateusz Brodowski[1], Marcin Kowalski[1], Marta Skwarecka[2], Katarzyna Pałka[3], Michał Skowicki[4], Anna Kula[4], Tomasz Lipiński[4], Anna Dettlaff[1], Mateusz Ficek[1], Jacek Ryl[1], Karolina Dziąbowska[3], Dawid Nidzworski[2,3] and Robert Bogdanowicz[1*]

[1] Gdańsk University of Technology, 11/12 G. Narutowicza St., 80-233, Gdańsk, Poland

[2] Institute of Biotechnology and Molecular Medicine, 3 Trzy Lipy St., 80-172, Gdańsk, Poland

[3] SensDx, 14b Postępu St., 02-676, Warszawa, Poland

[4] Łukasiewicz Research Network – PORT Polish Center for Technology Development, 147 Stabłowicka St., 54-066, Wrocław, Poland

***Corresponding author:** E-mail: rbogdan@eti.pg.edu.pl. Tel: +48-58-347-15-03. Fax: +48 58-347-18-48 (Robert Bogdanowicz)

Keywords: *Carbon Nanowalls, Electrochemical Impedance, Pathogen Detection, Haemophilus influenzae, Protein D*

Graphical Abstract:

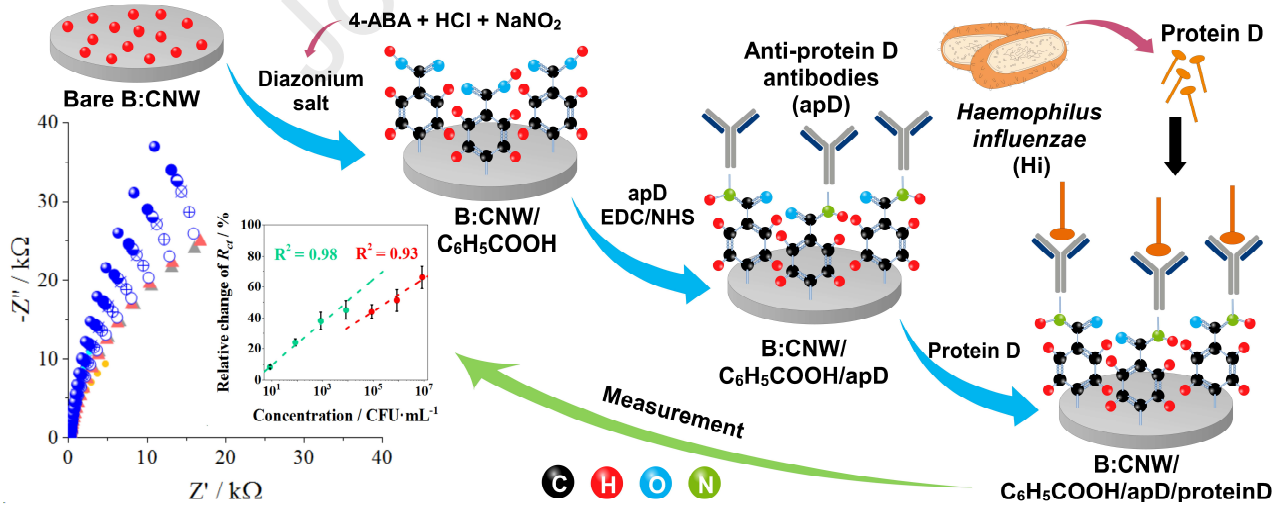

Abstract:

This study reports a novel impedimetric immunosensor for protein D detection in purified and bacterial (*Haemophilus influenzae*, Hi) samples. The detection was based on antigen recognition by anti-protein D antibodies (apD) immobilised at the maze-like boron-doped carbon nanowall

electrodes (B:CNW). The B:CNW electrodes were synthesised, and their surface was characterised by scanning electron microscopy (SEM) and X-ray photoelectron spectroscopy (XPS) methods. The sensor was prepared in a two-step procedure: apD were covalently linked on the previously modified B:CNW electrodes using diazonium salt. Modification steps were controlled by electrochemical impedance spectroscopy (EIS) and cyclic voltammetry (CV) measurements. The immunosensor exhibited excellent electrochemical performance, stability, satisfactory sensitivities, and linear ranges for antigen detection. *Protein D was detected down to 2.39×10^{2} fg/mL with a linear range extending from 3.37×10^{-11} to 3.37×10^{-3} µg/mL (in purified sample). Next, Hi's LOD was 5.20×10^{2} CFU/mL with a linear range of 8.39×10^{1}–8.39×10^{3} CFU/mL.* Selectivity studies showed no reaction with negative samples as *Streptococcus pyogenes, Streptococcus pneumoniae or Bordetella parapertussis* bacteria. Therefore, the new approach is suitable for rapid and quantitative detection of Hi, and is a good candidate for further tests on clinical samples.

1. Introduction

Haemophilus influenzae (Hi) is a Gram-negative bacterium found in human respiratory pathways. It is a commensal in the human nasopharynx, mainly present on the mucosal surfaces. This pathogen causes, *e.g.,* pneumonia, meningitis [1], and in the bloodstream, infections – septicemia, epiglottitis [2]. Hi isolates divide into encapsulated (six serotypes, a-f) and non-encapsulated. Protein D is a surface lipoprotein antigenically conserved and expressed by all 127 Hi strains; it is also involved in the pathogenesis of respiratory tract infections. Thus, Hi is a perfect target in the development of alternative detection methods, as well as in vaccine development [3–6].

The currently developed techniques for Hi determination are mainly molecular methods, *e.g.,* culture-based phenotypic identification [8], capsular genotyping [7,8], serotyping by agglutination [7,9], immunoglobulin analysis [10], immunochromatography [11,12], and PCR-based methods [13–15]. These methods are believed to be time-consuming and laborious. Rapid commercial tests are promising [16], however, they are not as popular as for other causatives of respiratory infections such as the influenza virus [17].

The biosensors field is not widely developed towards Hi detection. Only several methods are documented in the literature, which can be classified as new compared to the molecular methods. Takano *et al.* investigated loop-mediated isothermal amplification (LAMP), which is an isothermal version of standard PCR offering 1-10^{3}-fold greater sensitivity [18]. Swartz *et al.* investigated inductively coupled plasma-atomic emission spectroscopy for the detection of Hi type b capsular polysaccharide [19]. For electrochemical detection, Yadav *et al.* applied a square wave voltammetry method for chloramphenicol antibiotic detection using an aptamer-modified graphite electrode. The sensor was verified on different Hi strains to distinguish between drug-sensitive and drug-resistant ones [20].

Electrochemical biosensors (EBs) are promising tools for Hi detection due to their low-cost, high selectivity of detected analytes [21], and the possibility of miniaturisation [22]. EBs devices incorporate a biological recognition element such as, *e.g.*, antibodies [23], nucleic acids [24], proteins [25] that selectively react with the analyte. As a result, the biosensor provides specific

quantitative analytical information. Detection of the analyte can be performed by different electrochemical techniques: voltammetry [26], potentiometry [27], conductometry [28], amperometry [29], and electrochemical impedance spectroscopy [30].

Carbon nanomaterials such as carbon nanotubes [31–33], graphene [34–36], and graphene quantum dots [37] have attracted increasing interest as an electrode material for electrochemical biosensor application [38,39]. Carbon nanowalls are sp^2-rich phase nanostructures of aligned and well-separated graphene walls, which are good candidates for biosensor material due to their high surface-to-mass ratio and stability [40].

In this study, we demonstrate an electrochemical, impedimetric biosensor based on a maze-like boron-doped carbon nanowall (B:CNW) electrodes. The B:CNW electrodes were synthesised in a one-step growth process by microwave plasma-assisted chemical vapour deposition (CVD) using a gas mixture of H_2:CH_4:B_2H_6 and N_2. The presence of a boron dopant improves the charge transfer and electrochemical behaviour of carbon material when compared to typical carbon nanowalls [41–43]. The electrodes were modified in a two-step procedure by electroreduction of diazonium salt at the B:CNW surface and antibody immobilisation by zero-length cross-linkers.

The developed platform showed a highly sensitive and selective response to protein D and Hi. The achieved limit of detection is equal to 5.20×10^2 CFU/mL. To the best of the authors' knowledge, an electrochemical biosensor for *Haemophilus influenzae* detection has not been reported yet.

2. Materials and methods

2.1. Reagents

Potassium hexacyanoferrate(III), methanol, sodium nitrite, and hydrochloric acid were purchased from Chempur (Poland). Phosphate-buffered saline (PBS), 4-aminobenzoic acid, N-hydroxysuccinimide (NHS), 1-ethyl-3-(3-dimethylaminopropyl)-carbodiimide (EDC), and PCR primers were purchased from Sigma Aldrich (Germany). Hi *(*strain 51907), *S. pyogenes* (strain 700294), and *S. pneumoniae* (strain 700674) bacteria were purchased from ATCC (US). *B. parapertussis* bacteria (strain 529) were provided from the Polish Collection of Microorganisms. An ExtractMe DNA Bacteria kit was purchased from Blirt (Poland), and a SensiFAST SYBR No-ROX kit was purchased from Bioline (UK). All reagents were used without further purification. Aqueous solutions were made using double-distilled sterile water (ddH_2O).

2.2. Apparatus

PCR reactions were carried out in a CFX Connected Real-Time Thermocycler (Bio-Rad, US), and DNA concentrations were measured by a NanoDrop One (Thermo Scientific, UK). The morphology of the B:CNW was investigated by a SEM (S-3400N, HITACHI, Japan) with a tungsten source and variable chamber pressure. The XPS spectra of the pristine and modified B:CNW electrodes were measured using an Escalab 250Xi spectroscope (Thermo Fischer Scientific, UK) with a

monochromatic Al Kα source. The electrochemical measurements were performed using a potentiostat–galvanostat (VMP-300, Bio-Logic, France) under EC-Lab software.

2.3. Biomaterials preparation and identification by reference method

Nanobioengineering Laboratory produced mouse monoclonal antibodies at PORT Polish Center for Technology Development Ltd. by standard procedures as described in [44] with minor modifications. For detailed data, please see S2. Supplementary information.

Biotechnology Laboratory isolated recombinant protein D at the Institute of Biotechnology and Molecular Medicine following standard procedures. For detailed data, please see S2. Supplementary information. For the verification of the efficacy of produced antibodies, a control experiment was performed. The possibility of detection of *Haemophilus influenzae* protein D using anti-protein D antibodies was confirmed in the ELISA test (data not shown).

A single colony of *Hi*, *S. pyogenes*, *S. pneumoniae,* and *B. parapertussis* was inoculated in BHI broth (Sigma Aldrich), and cultured overnight at 37^{o}C. 1 mL of the overnight culture was centrifuged, and the cell pellet was resuspended in 1 mL of PBS Buffer.

A qPCR reaction detected the presence of the bacteria and their concentrations (CFU). Identification of Hi and *S. pneumoniae* was performed according to [45], and *S. pyogenes* and *B. parapertussis* according to [46] and [47], respectively. For detailed data, please see S2.4. Supplementary information.

2.4. Immunosensor fabrication

2.4.1. B:CNW electrode fabrication

The experimental setup used in this study has been described in detail elsewhere [48,49]. The samples were doped by using diborane (B_2H_6) as an acceptor precursor. The flow rates of H_2, CH_4, and B_2H_6 were kept at 287.5, 25, and 12.5 sccm, respectively, and the total gas pressure was 50 Torr. The typical microwave (2.45 GHz) power was 1300 W, and the substrate holder was heated using an induction heater to around 700°C. The B:CNW were grown on (100) oriented silicon substrates for 6 h, reaching thickness of 3 µm.

2.4.3. B:CNW electrode modification

A large set of B:CNW samples was tested and studied during the optimisation of process parameters to obtain an efficient modification procedure. Each surface was washed in an ultrasonic cleaner for 5 min in methanol and ddH_2O, and dried in an argon stream before the modification procedure. The detailed procedure of immunosensor fabrication and investigation are shown in Fig. 1.

The first step was the modification of bare B:CNW with diazonium salt to achieve B:CNW/C_6H_5COOH. The salt synthesis was carried out by dissolving 20 mg of 4-aminobenzoic acid

(ABA) in 2 mL of concentrated hydrochloric acid. Next, the mixture was cooled to 0 °C, and 2 mL of ddH_2O was added. An aqueous solution of sodium nitrite (25 mg in 3 mL ddH_2O) was added drop-by-drop to the cooled solution over 30 min. Subsequently, 250 µL of the freshly prepared diazonium salt solution was transported to an electrochemical cell, diluted twice with ddH_2O, and deaerated with argon for 5 min. Electrografting was carried out on B:CNW with a surface area of ca. 38.46 mm^2 (Ø7 mm), which was polarised 11 times from 0 to -1 V. Then, the electrode was washed with sterile ddH_2O.

The second step was the application of apD on the electrografted B:CNW/C_6H_5COOH to get B:CNW/C_6H_5COOH/apD. For this purpose, a solution of 34.5 mg EDC and 20.9 mg NHS in 5 mL PBS was prepared and stirred for 5 min at room temperature. In the meantime, a stock solution of apD was diluted 100-fold in PBS. Next, 40 µL of apD and 1 mL of carboxyl group activator (EDC/NHS) were mixed, and 50 µL of the obtained solution was applied on the B:CNW/C_6H_5COOH surface for 24 h at 4°C. After this time, the electrode was washed gently with ddH_2O, dried in argon, and stored in ambient conditions before use.

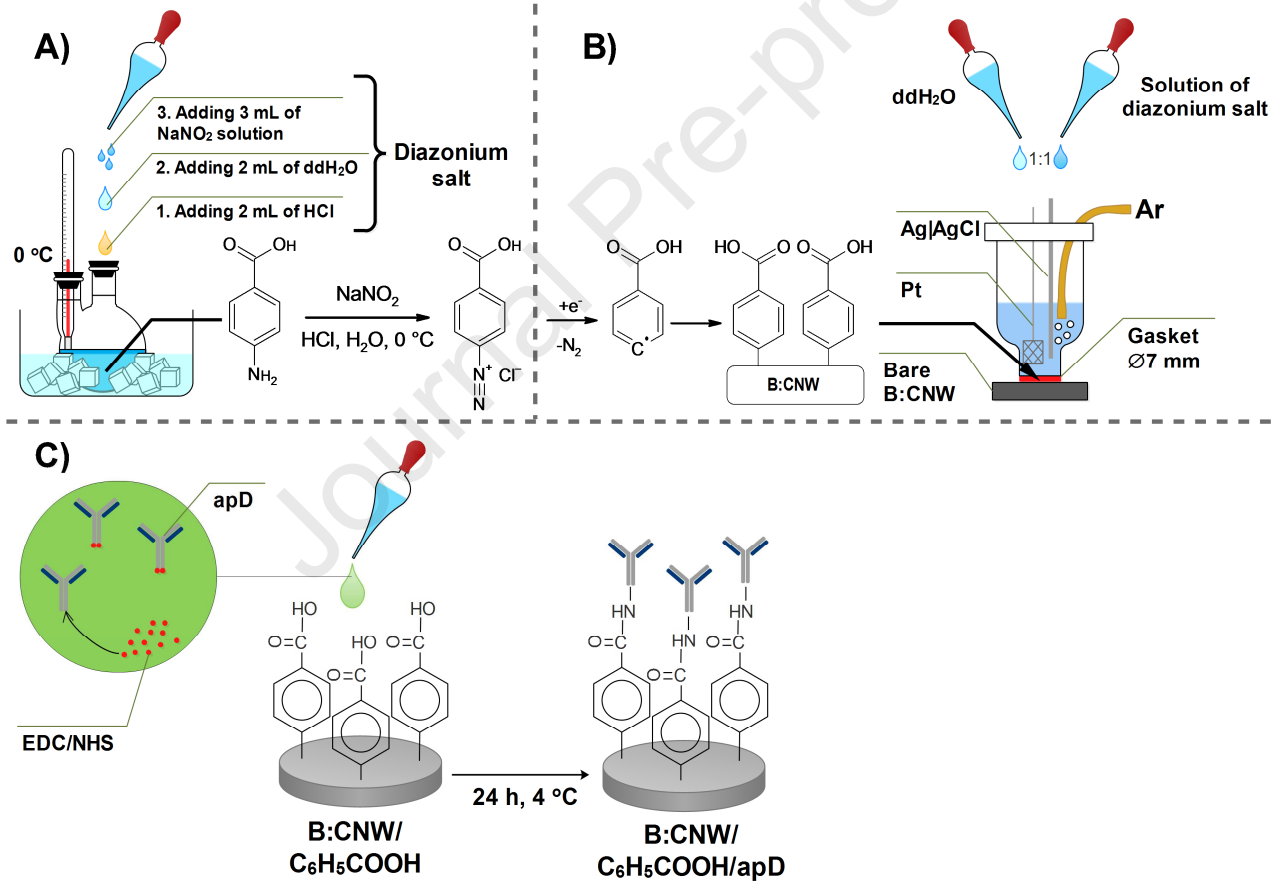

Fig. 1. Scheme of B:CNW electrode modification towards selective determination of Haemophilus influenzae (Hi) A) synthesis of a diazonium salt with its steps featured, B) electrografting of diazonium salt linkers at bare B:CNW surface using the electrochemical cell, C) antibody immobilization at carboxyl group of the 4-aminobenzoic acid modified B:CNW/C_6H_5COOH.

2.5. Electrochemical experiments

2.5.1. Measurements procedures

All measurements were carried out in a three-electrode system using a silver-chloride electrode (3 M KCl) as the reference electrode, a platinum grid as the counter electrode, and antibody-modified B:CNW/C_6H_5COOH/apD (ca. 19.62 mm^2, Ø5 mm surface area) as the working electrode. The supporting electrolyte was 1 mM $K_3[Fe(CN)_6]$ in 1×PBS pH 7.37. Before each measurement, the electrolyte (200 µL) was deaerated with argon for 5 min.

For the bare and modified B:CNW electrodes, the electrochemical impedance spectroscopy (EIS) and cyclic voltammetry (CV) measurements were carried out. The CV scan was in the potential range from -0.75 V to 0.75 V relative to the reference electrode at a scan rate of 50 mV/s, triplicate. On its basis, a formal oxidation potential of $[Fe(CN)_6]^{3-/4-}$ was determined for bare B:CNW, and then applied in EIS (3 min sample polarisation). The EIS measurement frequency range was 0.2 Hz – 10 kHz (52 points), stimulating the system with a single sinusoidal signal with a 10 mV amplitude.

3. Results

3.1. B:CNW surface characterisation

Scanning electron microscopy was applied for the investigation of the surface morphology of bare B:CNW (Fig. 2A). The obtained carbon nanowalls formed homogeneous, randomly vertically aligned maze-like structures with a wall-length of approximately 0.7 µm. The boron-doped carbon nanowall layer applied here exhibited a thickness of 3.2 µm, as reported previously in [50].

The XPS survey spectra of B:CNW and B:CNW/C_6H_5COOH (Fig. S1, Supplementary information) showed peaks of C 1s, N 1s, and O 1s at approximately 286 eV, 400 eV, and 532 eV, respectively. The high-resolution spectrum of the C 1s (Fig. 2C) was resolved into signals located in the range from 283.3 eV to 289.1 eV. The main peaks corresponded to the carbon-carbon -sp^2 and -sp^3 bonded at 284.3 eV and 284.9 eV. Next, the small C-B feature was observed at 283.4 eV [51–53]. The spectrum of the modified electrode also contained a signal from carbon from the carboxyl group at 289.1 eV. The N 1s signal (Fig. 2C) was fit using two peaks at 398.5 eV and 401.0 eV attributed to the chemical environments for pyridinic nitrogen (C-N-C) and quaternary nitrogen (N-$(C)_3$), respectively [54].

The deconvoluted O 1s spectrum (Fig. 2C) showed three component peaks at binding energies of 531.6 eV (C=O), and 533.2 eV (C-OH, C-O-C). The total oxygen content in the bare and modified B:CNW electrode differed significantly. The atomic concentration of O in the B:CNW was approximately 3.2%, whereas in the B:CNW/C_6H_5COOH, achieved 17.1%. The higher percentage of oxygen with a simultaneous decrease of the signal originating from the B:CNW electrode surface suggested successful attachment of -C_6H_5COOH moiety to the carbon nanowall surface. Thus, the XPS result coincides with the CV and EIS measurements. Curve fitting results of C 1s, O 1s, and N 1s XPS spectra of B:CNW and B:CNW/C_6H_5COOH were presented in Fig. 2B. The assignment of binding energy to the particular chemical bonds was done according to the literature [54–56].

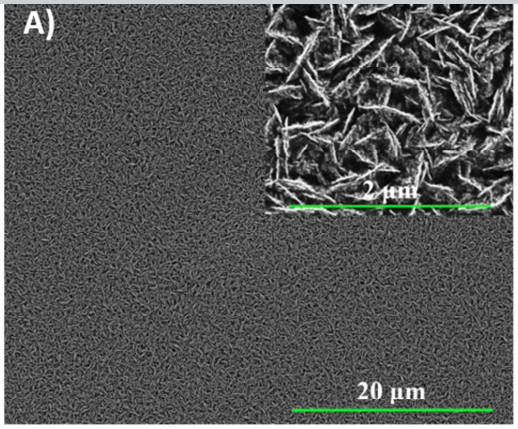

B)

	BE / eV	At% B:CNW	At% B:CNW/C_6H_5COOH	Assignment
C 1s	283.3 ± 0.1	3.3	1.0	C-B
	284.3	55.8	4.5	C=C (sp^2)
	284.9 ± 0.1	23.1	44.2	C-C (sp^3)
	286.0 ± 0.1	10.3	16.5	C-OH, C-O-C, C-N
	289.0	-	10.4	C=O
	∑ $C_{at\%}$	**92.5**	**76.6**	
O 1s	531.5 ± 0.1	1.7	6.4	C=O
	533.1 ± 0.1	1.5	10.7	C-OH, C-O-C
	∑ $O_{at\%}$	**3.2**	**17.1**	
N 1s	398.5 ± 0.1	1.9	1.7	C-N-C (pyridinic N)
	401.0	-	2.6	N-$(C)_3$ (quaternary N)
	∑ $N_{at\%}$	**1.9**	**4.3**	

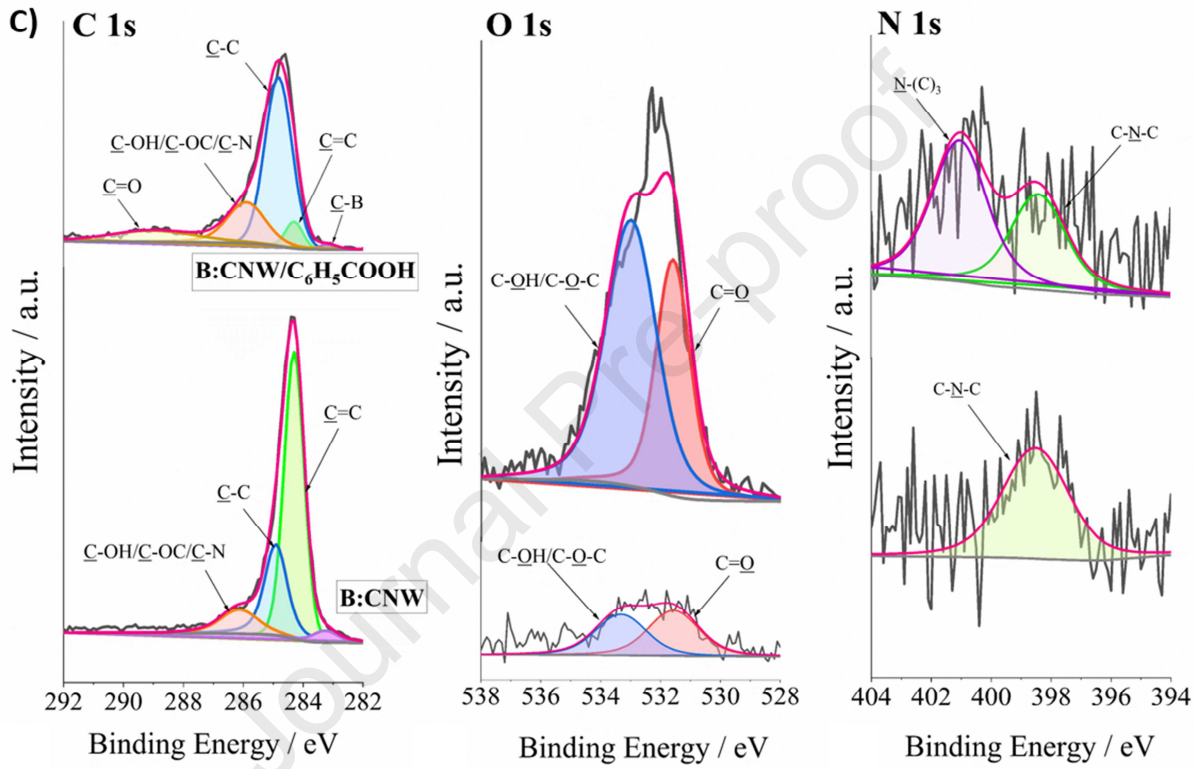

Fig. 2. Morphology and XPS studies of B:CNW surface modification: A) SEM micro-images of bare B:CNW surface taken with magnification of 2,500x (Inset A: image taken at 25,000x of magnification), B) Table with atomic % composition of bare B:CNW and modified B:CNW/C_6H_5COOH surfaces, C) High-resolution XPS C 1s, O 1s, and N 1s spectra for bare B:CNW (top) and B:CNW/C_6H_5COOH surfaces (bottom).

3.2. Electrochemical characterisation of immunosensor

To observe changes in the electrode properties during the modification steps, the CV and EIS techniques were used in accordance with the parameters from the Materials and methods section.

On the CV graph (Fig. 3A) for the bare B:CNW electrode, the oxidation and reduction peaks of $[Fe(CN)_6]^{4-}$ and $[Fe(CN)_6]^{3-}$ were well defined (heights of 120 µA·cm^{-2} each, potential difference not

exceeding 100 mV). The formal potential of $[Fe(CN)_6]^{3-/4-}$ for B:CNW was 0.15 V, and similar between electrodes. After the first stage of electrode modification, i.e., diazonium salt electrografting - B:CNW/C_6H_5COOH, the redox peaks were not observed, which indicated a high degree of surface coverage with p-carboxyphenyl groups. Next, the B:CNW/C_6H_5COOH electrode was incubated with the solution of EDC/NHS and apD. This step did not cause any noticeable CV changes as the B:CNW/C_6H_5COOH surface was previously blocked with deposited benzoic acid groups.

For the EIS data analysis (Fig. 3B), a an electric equivalent circuit was built (Fig. 3C), a derivative of Randles circuit with parallel capacitance replaced by the constant phase element (CPE). The CPE is the most often used to include representation of frequency dispersion due to material heterogeneity and overlapping of time constants. Its impedance, Z_{CPE}, is defined as $[Q(j\omega)]^{-n}$, where Q is heterogeneous quasi-capacitance in case of frequency dispersion effects and CPE exponent n is the so-called homogeneity factor (for α=1 CPE represents ideal capacitor) [57]. The main influence on the *quasi*-capacitance value has an electrochemically active surface, permeability, layer thickness as well as the degree of heterogeneity [58]. Furthermore, to represent the diffusion-controlled process, visible in the low-frequency range of the impedance spectra, a Warburg diffusion impedance element was introduced. The Z_W represents the diffusion of the electro-active species towards the electrode surface. In presence of barrier properties of diazonium salts film covering B:CNW electrode surface, the diffusion impedance is neglected, which is in good agreement with disappearance of redox peaks in CV scans.

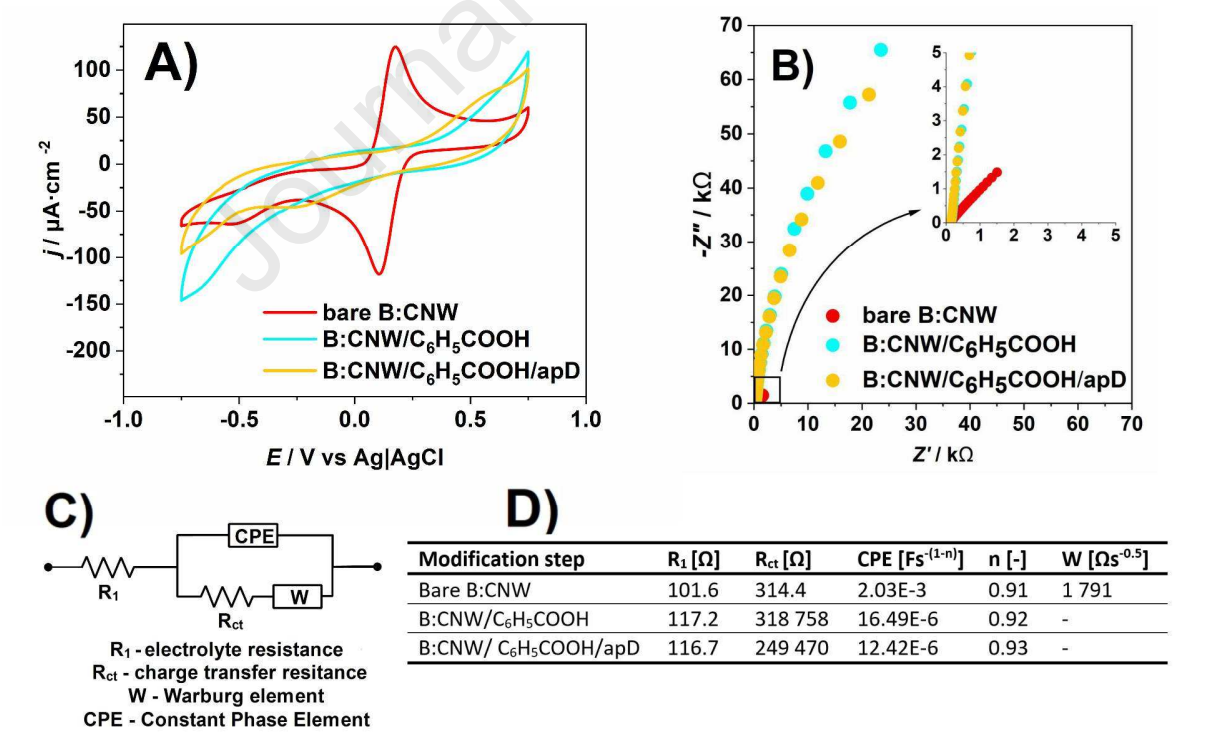

Modification step	R_1 [Ω]	R_{ct} [Ω]	CPE [$Fs^{-(1-n)}$]	n [-]	W [$\Omega s^{-0.5}$]
Bare B:CNW	101.6	314.4	2.03E-3	0.91	1 791
B:CNW/C_6H_5COOH	117.2	318 758	16.49E-6	0.92	-
B:CNW/ C_6H_5COOH/apD	116.7	249 470	12.42E-6	0.93	-

Fig. 3. Preparation of surface-modified B:CNW electrode: A) CV curves recorded for bare and modified B:CNW electrodes, B) EIS spectra of bare and modified B:CNW electrodes after incubation in different solutions recorded in 1 mM $K_3[Fe(CN)_6]$/ 1×PBS, C) applied electric

equivalent circuit (EEQC), D) list of values of elements calculated from applied EEQC for bare and modified B:CNW electrodes incubated in different solutions.

The two orders of magnitude decrease in the *quasi*-capacitance after electrografting indicates very effective adsorption of diazonium salt molecules onto the B:CNW surface, which corresponds well with the increase in the homogeneity parameter, also observed in impedance studies on organic functionalized layers by other authors [59]. Also, the increase in the R_{ct} parameter indicates a more difficult electron transfer process at the electrode surface, which was most likely caused by a reliable electrode coverage. After the electrode incubation with apD, a decrease in the resultant R_{ct} can be seen (about 70 kΩ less), which may be caused by partial hydrolysis of the adsorbed salt molecules. The changes in electrical circuit elements' values are presented in Fig. 3D.

Usually, the next step of immunosensor fabrication is to block unmodified sites on the electrode surface, *e.g.,* using bovine serum albumin (BSA) [60–62]. This is to prevent non-specific interactions between antigen and unmodified electrode sites [63]. In order to determine the validity of this treatment for a biosensor formed from B:CNW, the degree of electrode coverage after 24 h of incubation in the solution of apD and EDC/NHS was calculated using the relationship 1:

$$\theta = \frac{R_{ct,(1)} - R_{ct,(2)}}{R_{ct,(1)}} \times 100\ \%, \quad (1)$$

where θ is the electrode coverage degree, $R_{ct,(1)}$ and $R_{ct,(2)}$ are the R_{ct} for the modified and bare B:CNW, respectively. The θ value was 99.87%, which indicates an inconsiderable non-electrografted area of the electrode. The chance of non-specific adsorption on the electrode surface was assessed as very low; thus the stage of surface modification with BSA was omitted. Sensor selectivity tests later confirmed the correctness of this procedure.

3.3. Detection of bacterial protein D and sensor verification on *Haemophilus influenzae*

After B:CNW modification, it was placed in an electrochemical cell, and EIS spectra were recorded until system stabilisation was observed. The stability of the sensor was verified by two additions of PBS (20 µL) to exclude unspecific interactions. After the first verification of the accuracy of the modification procedure, the immunosensor was checked towards the target analyte – protein D deriving from Hi (samples were incubated for 5 min). Fig. 4A shows the impedance spectrum recorded during subsequent additions of the protein D solution with increasing concentrations, which was preceded by two-times additions of its solvent (PBS) as a negative control. The PBS additions gave a 12% response in first addition to the sample, and 3% between the next additions compared to further protein D additions (8% increase at first concentration of protein D and 20% in the next one). Further additions of the protein D solution caused a more pronounced increase in the total electron transfer resistance, and decrease in *quasi*-capacity as listed in Tables S1 and S2 (see S3.3. Supplementary information). The subsequent binding of protein D to the apD located on the electrode surface caused this phenomenon. An increase in the homogeneity of the surface, and thus an increase in the n parameter, were also achieved (Tables S1 and S2 in Supplementary information).

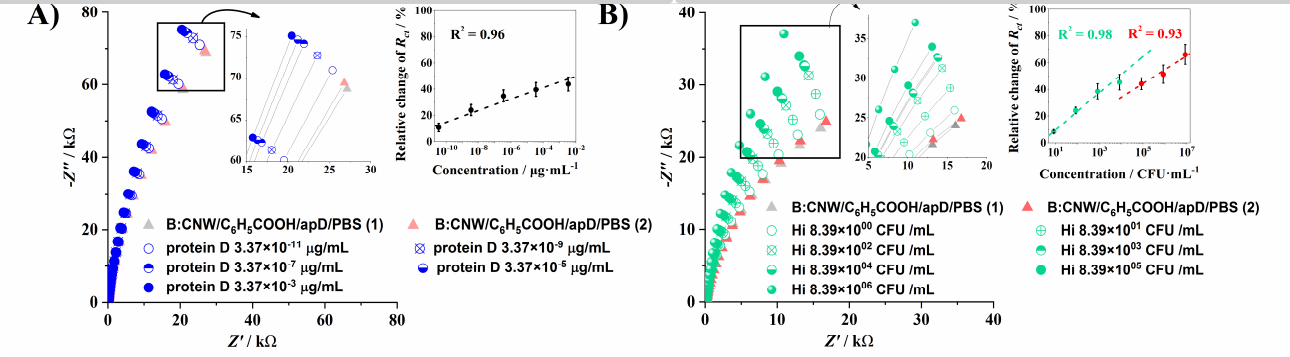

Fig. 4. *Detection of protein D and Haemophilus influenzae. Impedance spectra of B:CNW/C_6H_5COOH/apD electrodes incubated in PBS solutions with different: A) protein D concentrations derived from Hi, B) real Hi bacteria concentrations. Attn. Inset in A shows dependence of relative change of R_{ct} versus protein D concentration, while Inset in B displays relative shift in R_{ct} versus real Hi bacteria concentration.*

The calibration curve was constructed based on the obtained values. To unify these values, the degree of electrode coverage was used instead of the direct value of R_2 resistance, which was calculated using formula (1) where: $R_{ct,(2)}$ is the resistance for PBS, $R_{ct,(1)}$ is the resistance for the sample added. A similar procedure is also used in other works [63,64]. The obtained relationship is shown in Fig. 4A. Error bars were calculated as relative standard deviation (RSD), and their low values indicate very good repeatability of measurements. More information about the linearities and sensitivities of the biosensor is presented in section 3.5.

The success of the linearity response towards protein D classified the sensor for further studies on a real sample – Hi bacteria. The measurement and sample addition procedures were similar to protein D. Fig. 4B shows impedance spectra recorded for the Hi additions with increasing concentrations. Analogous changes were observed – a slight increase in R_{ct} resistance during the addition of PBS (3% between each other) and a more significant increase for Hi (24% for the concentration of 840 CFU/mL, for detailed data, please see Table S2, Supplementary information). It is worth noting that the increases in resistance are noticeably higher for Hi than protein D itself (66% for Hi, and 44% for protein D, and the highest concentrations). This is caused by the larger size of the bacteria, and the bigger amount of the target analyte, as one Hi particle has around 2800 protein D particles [5]. The resistance changes correlate very well with the increasing value of the n parameter, which indicates the degree of homogeneity of the electrode surface obtained in the case of bacterial adsorption than in the case of the protein itself. The graph of the concentration logarithm relationship to the system response was constructed analogously to the protein calibration curve, and is shown in Fig. 4B. Error bars calculated as RSD tend to increase at higher bacterial concentrations, which can be caused by different bacterial adsorption on the surface. With a much larger surface area, it is probably possible to hamper the adsorption process due to spherical hindrance, and thus a greater diversity of sensor responses. This phenomenon may become more and more critical in the case of a larger number of pathogens adsorbing on the surface.

3.4. Biosensor selectivity, repeatability and stability studies

S. pyogenes, S. pneumoniae, and *B. parapertussis* bacteria were used as potentially interfering bacteria to investigate the selectivity of the immunosensor. The selection was based on the causatives of respiratory tract infections, especially *S. pneumoniae* which is known as a common co-infection species with Hi [10,65]. The bacteria concentration was kept in the same order of magnitude to receive comparable results. Next, they were applied on the modified electrode separately and in mixtures (*B. parapertussis* with *S. pyogenes*, *B. parapertussis* with *S. pneumoniae*, and *S. pyogenes* with *S. pneumoniae*). After 5 min incubation, the EIS spectra were recorded. According to Fig. 5, all negative controls did not give substantial impedance increase, the percentage change of R_{ct} did not exceed 12 %, for both single and mixed samples, and this value was established as a threshold for the distinction between positive and negative samples. The small R_{ct} decrease in the case of two mixes (*B. parapertussis* with *S. pyogenes*, and *B. parapertussis* with *S. pneumoniae*) can be due to a high load of non-specific bacteria (concentration exceeding the order of magnitude of the Hi concentration), thus the rupture of the antibodies layer. The amount of *S. pyogenes* and *B. parapertussis* used in the assay is higher than in biological samples, according to [66,67]. Compared to the $\%R_{ct}$ change in the presence of positive Hi, the negative samples were proved to give no cross-reactivity, indicating that the proposed method has high selectivity for the detection of protein D in Hi bacteria.

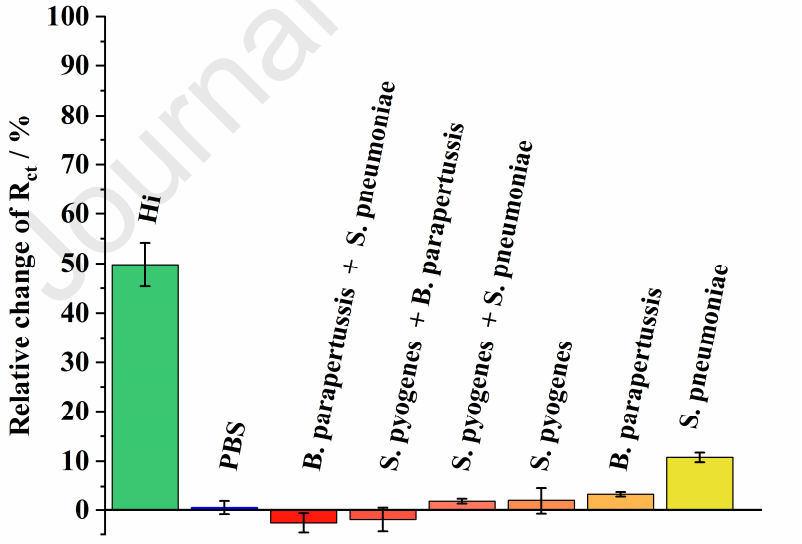

Fig. 5. The selectivity of the *B:CNW/C_6H_5COOH/apD* immunosensor tested versus positive Hi (4×10^4 CFU/mL) sample and other, mixed interfering pathogens: *B. parapertussis* (9×10^4 CFU/mL) + *S. pneumoniae* (4×10^4 CFU/mL), *S. pyogenes* (3×10^4 CFU/mL) + *B. parapertussis* (9×10^4 CFU/mL), *S. pyogenes* (3×10^4 CFU/mL) + *S. pneumoniae* (4×10^4 CFU/mL), *S. pyogenes* (6×10^4 CFU/mL), *B. parapertussis* (1×10^4 CFU/mL) and *S. pneumoniae* (8×10^4 CFU/mL). Attn. PBS bare buffer solution was shown as blank and reference sample.

The repeatability and reproducibility studies involved three independent sensors. Each electrode was freshly modified according to the optimised procedure and incubated with protein D for 5

min. The representative antigen concentration was 3.37×10^{-3} µg/mL. Next, triplicate impedimetric spectra were recorded, and RSD values were monitored. For repeatability, three replicates of measurement on one electrode resulted in an RDS value of 1.51%. The reproducibility between three biosensors prepared in the same conditions revealed an RSD value of 4.08%. The relatively low RSD values indicated satisfactory repeatability and reproducibility of the assay.

3.5. Comparison of sensitivities and linearity ranges

The calibration curve equation in general takes the form (2):

$$y = a(\ln(x)) + b, \quad (2)$$

For the protein D calibration curve, the linearity range covers all concentrations used (3.4×10^{-11} – 3.4×10^{-3}) µg/mL. In this case, the equation is expressed as follows: 1.76(ln(x)) + 56.94. In the case of dependence between sensor response and bacterial sample (Hi) concentration, two ranges of linearity are observed - first of 8.39×10^{1} – 8.39×10^{3} CFU/mL and second of 8.39×10^{4} – 8.39×10^{6})= CFU/mL. This phenomenon, not previously observed in other works, is probably closely related to the modification procedure used. The first bacterial concentrations bind specifically to active centers of antibodies (antigen-binding fragment (Fab) regions) on the electrode surface, which represents the first range of linearity. After exceeding a particular concentration of antigen, all free Fabs were saturated, giving the first linear characteristic of sensor response. The further addition of sample resulted in physical adsorption on the first layer of the bacteria associated with the antibodies. Thus the second linearity range was observed; however, deriving from not specific interaction. In this case, the first scope should be taken as the range in which the pathogen detection is specific, which is leading to equation: 5.42(ln(x)) – 1.18.

The detection limit was calculated using the method presented by Cebula *et al.* [63]. The highest response to the NEG sample (10.7 %, *S. pneumoniae*) was multiplied by 3, and LOD for both protein and bacteria was calculated from the obtained value by. The calculated values were 2.39×10^{2} fg/mL for protein D, respectively and 5.20×10^{2} CFU/mL for Hi.

Table 1. Comparison of parameters of previously reported detection methods of *Haemophilus influenzae* versus maze-like boron-doped carbon nanowall base immunosensor.

Detection method	Linearity range	LOD	Year	Ref.
Real-time PCR	1-10^{6} organisms per 25 µL reaction mixture	n/d*	2004	[9]
Real-time PCR	10^{3}-10^{7} CFU/mL	10^{3} CFU/mL	2015	[68]
PCR	n/d*	1.89×10^{3} DNA copies/µL	2018	[14]
PCR	n/d*	2.5×10^{3} cells/mL	2013	[69]
LAMP	10-10^{5} DNA copies per reaction mixture	10 DNA copies per reaction mixture	2017	[18]
Immunochromato-	n/d*	1×10^{6} CFU/mL	2017	[11]

graphic test strip				
This work	8.39×10^{1}–8.39×10^{3} CFU/mL	5.20×10^{2} CFU/mL	2020	-

*n/d – no data

Such high sensitivity was also manifested in other works, where the recognizing antibodies were grafted at the Si/SiO_2 electrode surface and interacting with analyte towards antigen α-fetoprotein detection. Maupas *et al.* revealed as low LOD as 1 ng/mL (15 pM) [70]. Next, the gold nanoparticles/multiwall carbon nanotube (MWCNT) electrodes manifested limit of detection of 7.4 ng/mL [71] during detection of human epidermal receptor 2 (HER2) by impedimetric technique. The MWCNT was attributed to deliver high conductivity, while Au nanoparticles are responsible for enhanced immobilization of receptors. Referred system is analogues to the reported here maze-like boron-doped carbon nanowall electrodes. Utilized carbon nanowalls reveal multiwall nature as shown previously in [72] contributing considerably to the conductivity and carrier mobility similarly to the above-mentioned MWCNT. Moreover, B:CNW electrodes showed boron-doped nanogranular diamond α-cluster inclusions, which are working as immobilization agents analogously to the Au nanoparticles decoration. This synergy allows, in specific cases, for extremely sensitive detection of proteins at picomolar concentration by EIS technique [73].

Wang *et al.* reported that increase of electro-active surface area by Au nanoparticles contribute to density of antigen immobilization. It enhances the number of sites, where antibody–antigen interaction takes place allowing for ultra-low LOD [74–76]. The high LOD of Hi observed at the maze-like B:CNW electrodes could be also directly attributed to large active area, thus resulting in large antigen payload and in consequence more with protein D molecules.

Furthermore, the comparable detection limit was achieved previously by Barreiros dos Santos *et al.* [77] reporting the detection and quantification of *E. coli* O157:H7 bacteria using EIS obtaining a limit of detection as low as 2 CFU/mL. We have used here in-direct approach for Hi detection by application protein D agent, which mimics determination of complete pathogen. Such a procedure enables much denser saturation of antibodies than in case of complete Hi binding. The lower size of protein D resulting into enhanced R_{ct} decrease, where the protein hindering effectively the transfer of redox probe towards the electrode surface. The charge of passivating protein D contributes also to the R_{ct} values delivering additional positive values near to the B:CNW surface [75]. Though, the effect of surface insulation induced by protein layer is the key factor modifying charge transfer resistance. Thus, the prior high density of antibodies amplify the variations of impedance output, boosting sensitivities to as low values as pg/mL [73].

Overall, the enzymatic reaction of antibody–antigen results in the side effect producing of insoluble compounds, which could also precipitate at the B:CNW surface [78]. This island-like film stimulates additionally impedance signal, similarly to the Au nanoparticles decoration amplifying immuno-reactions. The maze-like morphology with relatively similar inter-wall distances induces particular periodicity of biomolecules organization containing pinholes and nanopores where the small redox probe could be transferred thorough. The diffusion pathways of probe are modified

first by antigen attachment and later by protein D grafting. The interfacial electron-transfer is hindered by biofilm [79] recorded as shift of the Faradaic impedance spectra.

The key factor promoting the ultra-low LOD of presented system is the high specificity of applied here antigen-protein D system. It provides prompt and label-free response of pathogen detection to ensure the personal safety or deliver crucial evidence of hazard during screening processes [80].

Conclusions

In summary, we have reported the extended investigation of a novel impedimetric immunosensor for protein D detection. The recognition mechanism is based on the EIS spectra recorded at the antibody-modified boron-doped carbon nanowall surfaces. The developed immunosensor revealed excellent electrochemical performance along with large sensitivities and linear ranges for *Haemophilus influenzae* detection. The selectivity tests were negative to similar pathogens such as *Streptococcus pyogenes, Streptococcus pneumoniae*, and *Bordetella parapertussis*. The manifested high sensitivity and specificity is attributed to the hybrid diamond-graphene electrode surface showing high conductivity, the low double layer capacitance, and the large surface area inducing enhanced charge transfer electrode-solvent and the specific local stereochemistry of the linked antibodies.

In the near future, we plan to investigate the protocol for bacterial sample pretreatment to improve the proposed assay. The cell lysis will allow better access of the analyte to Fab regions of antibodies, and the sensor response will not be hindered due to the large size of the bacteria. We hope that this approach will result in lowering the currently achieved LOD for Hi bacteria, and will be suitable for clinical sample tests.

Acknowledgments

This work was supported by the National Centre for Research and Development (NCBR) TECHMATSTRATEG 1/347324/12/NCBR/2017.

Appendix A. Supplementary data

Supplementary data associated with this article can be found, in the online version, at doi: xxxx.

References:

[1] L.V. Michel, R. Kaur, M. Zavorin, K. Pryharski, M.N. Khan, C. LaClair, M. O'Neil, Q. Xu, M.E. Pichichero, Intranasal coinfection model allows for assessment of protein vaccines against nontypeable Haemophilus influenzae in mice, Journal of Medical Microbiology,. 67 (2018) 1527–1532. https://doi.org/10.1099/jmm.0.000827.

[2] A.-E. Deghmane, E. Hong, S. Chehboub, A. Terrade, M. Falguières, M. Sort, O. Harrison, K.A. Jolley, M.-K. Taha, High diversity of invasive Haemophilus influenzae isolates in France and the emergence of

resistance to third generation cephalosporins by alteration of ftsI gene, J. Infect. 79 (2019) 7–14. https://doi.org/10.1016/j.jinf.2019.05.007.
[3] M. Akkoyunlu, M. Ruan, A. Forsgren, Distribution of protein D, an immunoglobulin D-binding protein, in Haemophilus strains., Infect Immun. 59 (1991) 1231–1238.
[4] C. Clarke, L.O. Bakaletz, J. Ruiz-Guiñazú, D. Borys, T. Mrkvan, Impact of protein D-containing pneumococcal conjugate vaccines on non-typeable Haemophilus influenzae acute otitis media and carriage, Expert Review of Vaccines. 16 (2017) 751–764. https://doi.org/10.1080/14760584.2017.1333905.
[5] A. Forsgren, K. Riesbeck, Protein D of Haemophilus influenzae: A Protective Nontypeable H. influenzae Antigen and a Carrier for Pneumococcal Conjugate Vaccines, Clin Infect Dis. 46 (2008) 726–731. https://doi.org/10.1086/527396.
[6] T.M. Kilpi, J. Jokinen, T. Puumalainen, H. Nieminen, E. Ruokokoski, H. Rinta-Kokko, M. Traskine, P. Lommel, M. Moreira, J. Ruiz-Guinazu, D. Borys, L. Schuerman, A.A. Palmu, Effectiveness of pneumococcal Haemophilus influenzae protein D conjugate vaccine against pneumonia in children: A cluster-randomised trial, Vaccine. 36 (2018) 5891–5901. https://doi.org/10.1016/j.vaccine.2018.08.020.
[7] L.L. LaClaire, M.L.C. Tondella, D.S. Beall, C.A. Noble, P.L. Raghunathan, N.E. Rosenstein, T. Popovic, Active Bacterial Core Surveillance Team Members, Identification of Haemophilus influenzae serotypes by standard slide agglutination serotyping and PCR-based capsule typing, J. Clin. Microbiol. 41 (2003) 393–396. https://doi.org/10.1128/jcm.41.1.393-396.2003.
[8] C.C. Potts, N. Topaz, L.D. Rodriguez-Rivera, F. Hu, H.-Y. Chang, M.J. Whaley, S. Schmink, A.C. Retchless, A. Chen, E. Ramos, G.H. Doho, X. Wang, Genomic characterization of Haemophilus influenzae: a focus on the capsule locus, BMC Genomics. 20 (2019) 733. https://doi.org/10.1186/s12864-019-6145-8.
[9] A. Marty, O. Greiner, P.J.R. Day, S. Gunziger, K. Mühlemann, D. Nadal, Detection of Haemophilus influenzae Type b by Real-Time PCR, J Clin Microbiol. 42 (2004) 3813–3815. https://doi.org/10.1128/JCM.42.8.3813-3815.2004.
[10] M. Martinot, L. Oswald, E. Parisi, E. Etienne, N. Argy, I. Grawey, D.D. Briel, M.M. Zadeh, L. Federici, G. Blaison, C. Koebel, B. Jaulhac, Y. Hansmann, D. Christmann, Immunoglobulin deficiency in patients with Streptococcus pneumoniae or Haemophilus influenzae invasive infections, International Journal of Infectious Diseases. 19 (2014) 79–84. https://doi.org/10.1016/j.ijid.2013.10.020.
[11] M.M. Kong, B. Yang, C.J. Gong, H. Wang, X. Li, K.S. Zhao, J.J. Li, F. Wu, X. Liu, Z. Hu, Development of immunochromatographic colloidal gold test strip for rapid detection of Haemophilus influenzae in clinical specimens, J. Appl. Microbiol. 123 (2017) 287–294. https://doi.org/10.1111/jam.13489.
[12] Y. Tao, H. Hao, J. Li, M. Wang, Y. Wang, G. Zhang, Z. Hu, [Colloidal gold immunochromatographic strip for rapid detection of Haemophilus influenzae], Sheng Wu Gong Cheng Xue Bao. 35 (2019) 901–909. https://doi.org/10.13345/j.cjb.180428.
[13] G.M.K. Abdeldaim, B. Herrmann, PCR detection of Haemophilus influenzae from respiratory specimens, Methods Mol. Biol. 943 (2013) 115–123. https://doi.org/10.1007/978-1-60327-353-4_7.
[14] X. Fan, X. Liu, L. Ji, D. Cai, J. Jiang, J. Zhu, A. Sun, J. Yan, Epidemiological analysis and rapid detection by one-step multiplex PCR assay of Haemophilus influenzae in children with respiratory tract infections in Zhejiang Province, China, BMC Infectious Diseases. 18 (2018) 414. https://doi.org/10.1186/s12879-018-3295-2.
[15] L. Selva, R. Benmessaoud, M. Lanaspa, I. Jroundi, C. Moraleda, S. Acacio, M. Iñigo, A. Bastiani, M. Monsonis, R. Pallares, Q. Bassat, C. Muñoz-Almagro, Detection of Streptococcus pneumoniae and Haemophilus influenzae Type B by Real-Time PCR from Dried Blood Spot Samples among Children with Pneumonia: A Useful Approach for Developing Countries, PLOS ONE. 8 (2013) e76970. https://doi.org/10.1371/journal.pone.0076970.
[16] R.S. Daum, G.R. Siber, J.S. Kamon, R.R. Russell, Evaluation of a Commercial Latex Particle Agglutination Test for Rapid Diagnosis of Haemophilus influenzae Type b Infection, Pediatrics. 69 (1982) 466–471.
[17] S.V. Vemula, J. Zhao, J. Liu, X. Wang, S. Biswas, I. Hewlett, Current Approaches for Diagnosis of Influenza Virus Infections in Humans, Viruses. 8 (2016). https://doi.org/10.3390/v8040096.

[18] C. Takano, M. Seki, D.W. Kim, P.L. Kilgore, K. Fuwa, K. Takahashi, T. Inazaki, S. Hayakawa, Molecular Serotype-Specific Identification of Non-type b Haemophilus influenzae by Loop-Mediated Isothermal Amplification, Front. Microbiol. 8 (2017). https://doi.org/10.3389/fmicb.2017.01877.
[19] L.A. Swartz, J.J. Progar, J.C. May, The Determination of Phosphorus in Haemophilus influenzae Type b Conjugate Vaccines by Inductively Coupled Plasma-Atomic Emission Spectrometry, Biologicals. 28 (2000) 227–231. https://doi.org/10.1006/biol.2000.0261.
[20] S.K. Yadav, B. Agrawal, P. Chandra, R.N. Goyal, In vitro chloramphenicol detection in a Haemophilus influenza model using an aptamer-polymer based electrochemical biosensor, Biosens Bioelectron. 55 (2014) 337–342. https://doi.org/10.1016/j.bios.2013.12.031.
[21] É. Pardoux, A. Roux, R. Mathey, D. Boturyn, Y. Roupioz, Antimicrobial peptide arrays for wide spectrum sensing of pathogenic bacteria, Talanta. 203 (2019) 322–327. https://doi.org/10.1016/j.talanta.2019.05.062.
[22] N.J. Ronkainen, H.B. Halsall, W.R. Heineman, Electrochemical biosensors, Chem. Soc. Rev. 39 (2010) 1747–1763. https://doi.org/10.1039/B714449K.
[23] Y. Jia, Y. Li, S. Zhang, P. Wang, Q. Liu, Y. Dong, Mulberry-like Au@PtPd porous nanorods composites as signal amplifiers for sensitive detection of CEA, Biosensors and Bioelectronics. 149 (2020) 111842. https://doi.org/10.1016/j.bios.2019.111842.
[24] J. Yi, Z. Liu, J. Liu, H. Liu, F. Xia, D. Tian, C. Zhou, A label-free electrochemical aptasensor based on 3D porous CS/rGO/GCE for acetamiprid residue detection, Biosensors and Bioelectronics. 148 (2020) 111827. https://doi.org/10.1016/j.bios.2019.111827.
[25] J.O. Esteves-Villanueva, H. Trzeciakiewicz, S. Martic, A protein-based electrochemical biosensor for detection of tau protein, a neurodegenerative disease biomarker, Analyst. 139 (2014) 2823–2831. https://doi.org/10.1039/C4AN00204K.
[26] X. Zheng, L. Li, L. Zhang, L. Xie, X. Song, J. Yu, Multiple self-cleaning paper-based electrochemical ratiometric biosensor based on the inner reference probe and exonuclease III-assisted signal amplification strategy, Biosensors and Bioelectronics. 147 (2020) 111769. https://doi.org/10.1016/j.bios.2019.111769.
[27] K. Saeedfar, L.Y. Heng, T.L. Ling, M. Rezayi, Potentiometric Urea Biosensor Based on an Immobilised Fullerene-Urease Bio-Conjugate, Sensors. 13 (2013) 16851–16866. https://doi.org/10.3390/s131216851.
[28] T.P. Velychko, O.O. Soldatkin, V.G. Melnyk, S.V. Marchenko, S.K. Kirdeciler, B. Akata, A.P. Soldatkin, A.V. El'skaya, S.V. Dzyadevych, A Novel Conductometric Urea Biosensor with Improved Analytical Characteristic Based on Recombinant Urease Adsorbed on Nanoparticle of Silicalite, Nanoscale Research Letters. 11 (2016) 106. https://doi.org/10.1186/s11671-016-1310-3.
[29] Y. Song, T. Xu, J. Xiu, X. Zhang, Mini-pillar microarray for individually electrochemical sensing in microdroplets, Biosensors and Bioelectronics. 149 (2020) 111845. https://doi.org/10.1016/j.bios.2019.111845.
[30] M. Kim, R.J. Iezzi, B.S. Shim, D.C. Martin, Impedimetric Biosensors for Detecting Vascular Endothelial Growth Factor (VEGF) Based on Poly(3,4-ethylene dioxythiophene) (PEDOT)/Gold Nanoparticle (Au NP) Composites, Front. Chem. 7 (2019). https://doi.org/10.3389/fchem.2019.00234.
[31] H. Karimi-Maleh, F. Tahernejad-Javazmi, A.A. Ensafi, R. Moradi, S. Mallakpour, H. Beitollahi, A high sensitive biosensor based on FePt/CNTs nanocomposite/N-(4-hydroxyphenyl)-3,5-dinitrobenzamide modified carbon paste electrode for simultaneous determination of glutathione and piroxicam, Biosens Bioelectron. 60 (2014) 1–7. https://doi.org/10.1016/j.bios.2014.03.055.
[32] Y. Plekhanova, S. Tarasov, A. Bykov, N. Prisyazhnaya, V. Kolesov, V. Sigaev, M.A. Signore, A. Reshetilov, Multiwalled Carbon Nanotubes and the Electrocatalytic Activity of Gluconobacter oxydans as the Basis of a Biosensor, Biosensors (Basel). 9 (2019). https://doi.org/10.3390/bios9040137.
[33] T.-T. Tran, K. Clark, W. Ma, A. Mulchandani, Detection of a secreted protein biomarker for citrus Huanglongbing using a single-walled carbon nanotubes-based chemiresistive biosensor, Biosensors and Bioelectronics. 147 (2020) 111766. https://doi.org/10.1016/j.bios.2019.111766.
[34] N. Chauhan, T. Maekawa, D.N.S. Kumar, Graphene based biosensors—Accelerating medical diagnostics to new-dimensions, Journal of Materials Research. 32 (2017) 2860–2882. https://doi.org/10.1557/jmr.2017.91.

[35] E. Morales-Narváez, L. Baptista-Pires, A. Zamora-Gálvez, A. Merkoçi, Graphene-Based Biosensors: Going Simple, Advanced Materials. 29 (2017) 1604905. https://doi.org/10.1002/adma.201604905.
[36] M. Pumera, Graphene in biosensing, Materials Today. 14 (2011) 308–315. https://doi.org/10.1016/S1369-7021(11)70160-2.
[37] H. Mahmoudi-Moghaddam, S. Tajik, H. Beitollahi, A new electrochemical DNA biosensor based on modified carbon paste electrode using graphene quantum dots and ionic liquid for determination of topotecan, Microchemical Journal. 150 (2019) 104085. https://doi.org/10.1016/j.microc.2019.104085.
[38] E.P. Simão, D.B.S. Silva, M.T. Cordeiro, L.H.V. Gil, C.A.S. Andrade, M.D.L. Oliveira, Nanostructured impedimetric lectin-based biosensor for arboviruses detection, Talanta. 208 (2020) 120338. https://doi.org/10.1016/j.talanta.2019.120338.
[39] R. Nazari-Vanani, H. Heli, N. Sattarahmady, An impedimetric genosensor for Leishmania infantum based on electrodeposited cadmium sulfide nanosheets, Talanta. 217 (2020) 121080. https://doi.org/10.1016/j.talanta.2020.121080.
[40] A. Vesel, R. Zaplotnik, G. Primc, M. Mozetič, Synthesis of Vertically Oriented Graphene Sheets or Carbon Nanowalls—Review and Challenges, Materials (Basel). 12 (2019). https://doi.org/10.3390/ma12182968.
[41] M. Pierpaoli, M. Ficek, M. Rycewicz, M. Sawczak, J. Karczewski, M.L. Ruello, R. Bogdanowicz, Tailoring Electro/Optical Properties of Transparent Boron-Doped Carbon Nanowalls Grown on Quartz, Materials. 12 (2019) 547. https://doi.org/10.3390/ma12030547.
[42] K.J. Sankaran, M. Ficek, S. Kunuku, K. Panda, C.-J. Yeh, J.Y. Park, M. Sawczak, P.P. Michałowski, K.-C. Leou, R. Bogdanowicz, I.-N. Lin, K. Haenen, Self-organized multi-layered graphene–boron-doped diamond hybrid nanowalls for high-performance electron emission devices, Nanoscale. 10 (2018) 1345–1355. https://doi.org/10.1039/C7NR06774G.
[43] M. Sobaszek, K. Siuzdak, J. Ryl, M. Sawczak, S. Gupta, S.B. Carrizosa, M. Ficek, B. Dec, K. Darowicki, R. Bogdanowicz, Diamond Phase (sp3-C) Rich Boron-Doped Carbon Nanowalls (sp2-C): Physicochemical and Electrochemical Properties, J. Phys. Chem. C. 121 (2017) 20821–20833. https://doi.org/10.1021/acs.jpcc.7b06365.
[44] P. Holzlöhner, K. Hanack, Generation of Murine Monoclonal Antibodies by Hybridoma Technology, J Vis Exp. (2017). https://doi.org/10.3791/54832.
[45] C.E. Corless, M. Guiver, R. Borrow, V. Edwards-Jones, A.J. Fox, E.B. Kaczmarski, Simultaneous detection of Neisseria meningitidis, Haemophilus influenzae, and Streptococcus pneumoniae in suspected cases of meningitis and septicemia using real-time PCR, J. Clin. Microbiol. 39 (2001) 1553–1558. https://doi.org/10.1128/JCM.39.4.1553-1558.2001.
[46] D. Liu, S. Hollingshead, E. Swiatlo, M.L. Lawrence, F.W. Austin, Rapid identification of Streptococcus pyogenes with PCR primers from a putative transcriptional regulator gene, Res. Microbiol. 156 (2005) 564–567. https://doi.org/10.1016/j.resmic.2005.01.010.
[47] M.E. Castillo, C. Bada, O. Del Aguila, V. Petrozzi-Helasvuo, V. Casabona-Ore, I. Reyes, J. Del Valle-Mendoza, Detection of Bordetella pertussis using a PCR test in infants younger than one year old hospitalized with whooping cough in five Peruvian hospitals, Int. J. Infect. Dis. 41 (2015) 36–41. https://doi.org/10.1016/j.ijid.2015.10.020.
[48] M. Ficek, R. Bogdanowicz, J. Ryl, Nanocrystalline CVD Diamond Coatings on Fused Silica Optical Fibres: Optical Properties Study, Acta Physica Polonica A. 127 (2015) 868–873. https://doi.org/10.12693/APhysPolA.127.868.
[49] I.S. Hosu, M. Sobaszek, M. Ficek, R. Bogdanowicz, H. Drobecq, L. Boussekey, A. Barras, O. Melnyk, R. Boukherroub, Y. Coffinier, Carbon nanowalls: a new versatile graphene based interface for the laser desorption/ionization-mass spectrometry detection of small compounds in real samples, Nanoscale. 9 (2017) 9701–9715. https://doi.org/10.1039/C7NR01069A.
[50] K. Siuzdak, M. Ficek, M. Sobaszek, J. Ryl, M. Gnyba, P. Niedziałkowski, N. Malinowska, J. Karczewski, R. Bogdanowicz, Boron-Enhanced Growth of Micron-Scale Carbon-Based Nanowalls: A Route toward High Rates of Electrochemical Biosensing, ACS Appl Mater Interfaces. 9 (2017) 12982–12992. https://doi.org/10.1021/acsami.6b16860.

[51] D. Banerjee, K.J. Sankaran, S. Deshmukh, M. Ficek, G. Bhattacharya, J. Ryl, D.M. Phase, M. Gupta, R. Bogdanowicz, I.-N. Lin, A. Kanjilal, K. Haenen, S.S. Roy, 3D Hierarchical Boron-Doped Diamond-Multilayered Graphene Nanowalls as an Efficient Supercapacitor Electrode, J. Phys. Chem. C. 123 (2019) 15458–15466. https://doi.org/10.1021/acs.jpcc.9b03628.
[52] K.J. Sankaran, M. Ficek, K. Panda, C.-J. Yeh, M. Sawczak, J. Ryl, K.-C. Leou, J.Y. Park, I.-N. Lin, R. Bogdanowicz, K. Haenen, Boron-Doped Nanocrystalline Diamond–Carbon Nanospike Hybrid Electron Emission Source, ACS Appl. Mater. Interfaces. 11 (2019) 48612–48623. https://doi.org/10.1021/acsami.9b17942.
[53] D. Banerjee, K.J. Sankaran, S. Deshmukh, M. Ficek, C.-J. Yeh, J. Ryl, I.-N. Lin, R. Bogdanowicz, A. Kanjilal, K. Haenen, S.S. Roy, Single-step grown boron doped nanocrystalline diamond-carbon nanograss hybrid as an efficient supercapacitor electrode, Nanoscale. 12 (2020) 10117–10126. https://doi.org/10.1039/D0NR00230E.
[54] R. Atchudan, T.N.J.I. Edison, K.R. Aseer, S. Perumal, N. Karthik, Y.R. Lee, Highly fluorescent nitrogen-doped carbon dots derived from Phyllanthus acidus utilized as a fluorescent probe for label-free selective detection of Fe3+ ions, live cell imaging and fluorescent ink, Biosens Bioelectron. 99 (2018) 303–311. https://doi.org/10.1016/j.bios.2017.07.076.
[55] D. Banerjee, K.J. Sankaran, S. Deshmukh, M. Ficek, G. Bhattacharya, J. Ryl, D.M. Phase, M. Gupta, R. Bogdanowicz, I.-N. Lin, A. Kanjilal, K. Haenen, S.S. Roy, 3D Hierarchical Boron-Doped Diamond-Multilayered Graphene Nanowalls as an Efficient Supercapacitor Electrode, J. Phys. Chem. C. 123 (2019) 15458–15466. https://doi.org/10.1021/acs.jpcc.9b03628.
[56] A. Dettlaff, M. Sawczak, E. Klugmann-Radziemska, D. Czylkowski, R. Miotk, M. Wilamowska-Zawłocka, High-performance method of carbon nanotubes modification by microwave plasma for thin composite films preparation, RSC Adv. 7 (2017) 31940–31949. https://doi.org/10.1039/C7RA04707J.
[57] J. Wysocka, M. Cieslik, S. Krakowiak, J. Ryl, Carboxylic acids as efficient corrosion inhibitors of aluminium alloys in alkaline media, Electrochimica Acta. 289 (2018) 175–192. https://doi.org/10.1016/j.electacta.2018.08.070.
[58] J. Ryl, M. Brodowski, M. Kowalski, W. Lipinska, P. Niedzialkowski, J. Wysocka, Corrosion Inhibition Mechanism and Efficiency Differentiation of Dihydroxybenzene Isomers Towards Aluminum Alloy 5754 in Alkaline Media, Materials. 12 (2019) 3067. https://doi.org/10.3390/ma12193067.
[59] R.K. Shervedani, S.A. Mozaffari, Impedimetric sensing of uranyl ion based on phosphate functionalized cysteamine self-assembled monolayers, Analytica Chimica Acta. 562 (2006) 223–228. https://doi.org/10.1016/j.aca.2006.01.046.
[60] A.O. Idris, N. Mabuba, O.A. Arotiba, An alpha-fetoprotein electrochemical immunosensor based on a carbon/gold bi-nanoparticle platform, Anal. Methods. 10 (2018) 5649–5658. https://doi.org/10.1039/C8AY02360C.
[61] P. Samadi Pakchin, H. Ghanbari, R. Saber, Y. Omidi, Electrochemical immunosensor based on chitosan-gold nanoparticle/carbon nanotube as a platform and lactate oxidase as a label for detection of CA125 oncomarker, Biosensors and Bioelectronics. 122 (2018) 68–74. https://doi.org/10.1016/j.bios.2018.09.016.
[62] H. Xiang, Y. Wang, M. Wang, Y. Shao, Y. Jiao, Y. Zhu, A redox cycling-amplified electrochemical immunosensor for α-fetoprotein sensitive detection via polydopamine nanolabels, Nanoscale. 10 (2018) 13572–13580. https://doi.org/10.1039/C8NR02946F.
[63] Z. Cebula, S. Żołędowska, K. Dziąbowska, M. Skwarecka, N. Malinowska, W. Białobrzeska, E. Czaczyk, K. Siuzdak, M. Sawczak, R. Bogdanowicz, D. Nidzworski, Detection of the Plant Pathogen Pseudomonas Syringae pv. Lachrymans on Antibody-Modified Gold Electrodes by Electrochemical Impedance Spectroscopy, Sensors. 19 (2019) 5411. https://doi.org/10.3390/s19245411.
[64] J. Wan, J. Ai, Y. Zhang, X. Geng, Q. Gao, Z. Cheng, Signal-off impedimetric immunosensor for the detection of Escherichia coli O157:H7, Scientific Reports. 6 (2016) 19806. https://doi.org/10.1038/srep19806.
[65] K.E.D. Weimer, C.E. Armbruster, R.A. Juneau, W. Hong, B. Pang, W.E. Swords, Coinfection with Haemophilus influenzae promotes pneumococcal biofilm formation during experimental otitis media and impedes the progression of pneumococcal disease, J. Infect. Dis. 202 (2010) 1068–1075. https://doi.org/10.1086/656046.

[66] L. Brodsky, L. Moore, J.F. Stanievich, P.L. Ogra, The immunology of tonsils in children: the effect of bacterial load on the presence of B- and T-cell subsets, Laryngoscope. 98 (1988) 93–98. https://doi.org/10.1288/00005537-198801000-00019.
[67] Y. Nakamura, K. Kamachi, H. Toyoizumi-Ajisaka, N. Otsuka, R. Saito, J. Tsuruoka, T. Katsuta, N. Nakajima, K. Okada, T. Kato, Y. Arakawa, Marked difference between adults and children in Bordetella pertussis DNA load in nasopharyngeal swabs, Clin. Microbiol. Infect. 17 (2011) 365–370. https://doi.org/10.1111/j.1469-0691.2010.03255.x.
[68] F. Safaeyan, M.R. Nahaei, S.J. Seifi, H.S. Kafil, J. Sadeghi, Quantitative detection of Staphylococcus aureus, Streptococcus pneumoniae and Haemophilus influenzae in patients with new influenza A (H1N1)/2009 and influenza A/2010 virus infection, GMS Hyg Infect Control. 10 (2015) Doc06. https://doi.org/10.3205/dgkh000249.
[69] K.M. Hare, R.L. Marsh, M.J. Binks, K. Grimwood, S.J. Pizzutto, A.J. Leach, A.B. Chang, H.C. Smith-Vaughan, Quantitative PCR confirms culture as the gold standard for detection of lower airway infection by nontypeable Haemophilus influenzae in Australian Indigenous children with bronchiectasis, Journal of Microbiological Methods. 92 (2013) 270–272. https://doi.org/10.1016/j.mimet.2012.12.013.
[70] H. Maupas, C. Saby, C. Martelet, N. Jaffrezic-Renault, A.P. Soldatkin, M.-H. Charles, T. Delair, B. Mandrand, Impedance analysis of Si/SiO2 heterostructures grafted with antibodies: an approach for immunosensor development, Journal of Electroanalytical Chemistry. 406 (1996) 53–58. https://doi.org/10.1016/0022-0728(95)04443-4.
[71] E. Arkan, R. Saber, Z. Karimi, M. Shamsipur, A novel antibody–antigen based impedimetric immunosensor for low level detection of HER2 in serum samples of breast cancer patients via modification of a gold nanoparticles decorated multiwall carbon nanotube-ionic liquid electrode, Analytica Chimica Acta. 874 (2015) 66–74. https://doi.org/10.1016/j.aca.2015.03.022.
[72] K.J. Sankaran, M. Ficek, S. Kunuku, K. Panda, C.-J. Yeh, J.Y. Park, M. Sawczak, P.P. Michałowski, K.-C. Leou, R. Bogdanowicz, I.-N. Lin, K. Haenen, Self-organized multi-layered graphene–boron-doped diamond hybrid nanowalls for high-performance electron emission devices, Nanoscale. 10 (2018) 1345–1355. https://doi.org/10.1039/C7NR06774G.
[73] E. Prats-Alfonso, X. Sisquella, N. Zine, G. Gabriel, A. Guimerà, F.J. del Campo, R. Villa, A.H. Eisenberg, M. Mrksich, A. Errachid, J. Aguiló, F. Albericio, Cancer Prognostics by Direct Detection of p53-Antibodies on Gold Surfaces by Impedance Measurements, Small. 8 (2012) 2106–2115. https://doi.org/10.1002/smll.201102724.
[74] M. Wang, L. Wang, G. Wang, X. Ji, Y. Bai, T. Li, S. Gong, J. Li, Application of impedance spectroscopy for monitoring colloid Au-enhanced antibody immobilization and antibody–antigen reactions, Biosensors and Bioelectronics. 19 (2004) 575–582. https://doi.org/10.1016/S0956-5663(03)00252-5.
[75] P. Jolly, N. Formisano, J. Tkáč, P. Kasák, C.G. Frost, P. Estrela, Label-free impedimetric aptasensor with antifouling surface chemistry: A prostate specific antigen case study, Sensors and Actuators B: Chemical. 209 (2015) 306–312. https://doi.org/10.1016/j.snb.2014.11.083.
[76] Y. Xiao, C.M. Li, Y. Liu, Electrochemical impedance characterization of antibody–antigen interaction with signal amplification based on polypyrrole–streptavidin, Biosensors and Bioelectronics. 22 (2007) 3161–3166. https://doi.org/10.1016/j.bios.2007.02.008.
[77] M. Barreiros dos Santos, J.P. Agusil, B. Prieto-Simón, C. Sporer, V. Teixeira, J. Samitier, Highly sensitive detection of pathogen Escherichia coli O157:H7 by electrochemical impedance spectroscopy, Biosensors and Bioelectronics. 45 (2013) 174–180. https://doi.org/10.1016/j.bios.2013.01.009.
[78] F. Patolsky, M. Zayats, E. Katz, I. Willner, Precipitation of an Insoluble Product on Enzyme Monolayer Electrodes for Biosensor Applications: Characterization by Faradaic Impedance Spectroscopy, Cyclic Voltammetry, and Microgravimetric Quartz Crystal Microbalance Analyses, Anal. Chem. 71 (1999) 3171–3180. https://doi.org/10.1021/ac9901541.
[79] J. Sopoušek, J. Věžník, P. Skládal, K. Lacina, Blocking the Nanopores in a Layer of Nonconductive Nanoparticles: Dominant Effects Therein and Challenges for Electrochemical Impedimetric Biosensing, ACS Appl. Mater. Interfaces. 12 (2020) 14620–14628. https://doi.org/10.1021/acsami.0c02650.

[80] F.O. K Owino, O.A. Sadik, Impedance Spectroscopy: A Powerful Tool for Rapid Biomolecular Screening and Cell Culture Monitoring, Electroanalysis. 17 (2005) 2101–2113. https://doi.org/10.1002/elan.200503371.

Highlights:

- Impedimetric immunosensor for detection of *Haemophilus influenzae (Hi)* protein D.
- Specific anti-protein D antibody immobilisation at a maze-like nanowall (B:CNW) electrodes.
- High selectivity of the immunosensor towards protein D and Hi bacteria.
- The LOD of Haemophilus influenzae bacteria is 5.20×10^2 CFU/mL.

Mateusz Brodowski : Conceptualization, Methodology, Visualization, Writing - Review & Editing

Marcin Kowalski: Conceptualization, Methodology, Visualization, Writing - Original Draft

Marta Skwarecka: Methodology, Investigation, Writing - Original Draft

Katarzyna Pałka: Resources, Writing - Original Draft

Michał Skowicki: Conceptualization, Visualization

Anna Kula: Conceptualization, Visualization

Tomasz Lipiński: Conceptualization, Visualization

Anna Dettlaff: Investigation, Data Curation, Visualization, Writing - Original Draft

Mateusz Ficek: Investigation, Data Curation, Writing - Original Draft

Jacek Ryl: Investigation, Data Curation,

Karolina Dziąbowska: Conceptualization, Project administration, Writing - Review & Editing

Dawid Nidzworski : Project administration, Funding acquisition

Robert Bogdanowicz: Visualization, Validation, Project administration, Funding acquisition, Supervision, Writing - Review & Editing

Declaration of interests

☒ The authors declare that they have no known competing financial interests or personal relationships that could have appeared to influence the work reported in this paper.

☐The authors declare the following financial interests/personal relationships which may be considered as potential competing interests:

Robert Bogdanowicz